Semi-automatic Segmentation of Fractured Pelvic Bones for Surgical Planning

Jürgen Fornaro[1], Gábor Székely[2], and Matthias Harders[2]

[1] Institute of Diagnostic Radiology, University Hospital Zurich
juergen.fornaro@usz.ch
[2] Computer Vision Lab, ETH Zurich
Switzerland
{mharders,szekely}@vision.ee.ethz.ch

Abstract. The segmentation of bones and bone fragments in clinical computed tomography datasets is an important first step in order to carry out computer-based surgical planning using patient-specific anatomical models. While semi-automatic and automatic methods have been proposed for the intact pelvic bone, the segmentation of bone fragments in the fractured pelvic bone still is a challenge due to weak boundaries and the diversity of injury patterns. We propose a semi-automatic multi-step segmentation method using bone and fracture gap enhancement filtering and a graph cut based bone fragment separation approach. The key contribution is a technique for automated detection of incorrect bone fragment separation in the case of incomplete pelvic fractures based on fracture gap planes detected in Hessian filtered images. Moreover, we propose a new sheetness measure based on a modified Hessian matrix. Our system is capable of segmenting fragments of complex hip fractures with only minimal user interaction.

Keywords: Bone segmentation, fractures, surgical planning.

1 Introduction

In our current research we focus on applying simulation techniques for treatment planning in acetabular fractures. These fractures are among the most challenging ones to treat in clinical practice. They typically occur as a result of high-energy traumas such as motor vehicle accidents or falls from a height [1], or less often as a consequence of minor traumas in older patients with osteopenic bone [2]. The anatomy of the pelvis is extremely complex. Moreover, pelvic fractures are diverse and relatively rare, such that patient-individual treatment is often mandatory.

Surgery planning tools for acetabular fracture reduction and fixation have been shown to increase reduction accuracy and to reduce operation times [3, 4]. Advanced simulation-based systems support the adaptation of different types and sizes of osteosynthesis implants to the reduced pelvis as well as mechanical tests of potential intervention plans [5]. For instance, screw trajectories should penetrate fracture gaps at about 90 degrees to prevent displacement of the bone fragments while tightening the

F. Bello and S. Cotin (Eds.): ISBMS 2010, LNCS 5958, pp. 82–89, 2010.

screw. This implies that models used for pelvic surgery planning should comprise the cortical as well as the cancellous bone.

In order to carry out computer-based surgical planning, triangular surface meshes of fracture fragments have to be obtained. To this end, appropriate segmentations are required. Simple automatic methods such as thresholding are not sufficient for obtaining these, while manual segmentations are tedious and time-intensive.

Therefore, we have developed a hybrid multi-step pipeline for the semi-automatic segmentation of the fractured pelvic bone as well as the proximal femora, based on clinically obtained CT datasets. The key contribution of our work is a technique for automated detection of incorrect bone fragment separation in the case of incomplete pelvic fractures. Fracture gap planes are detected in Hessian filtered images using an optimized Ransac algorithm. Moreover, we propose a new sheetness measure based on a modified Hessian matrix. Our system is capable of segmenting fragments of complex hip fractures with only minimal user interaction. The obtained segmentations are used as input to our fracture treatment planning software [5].

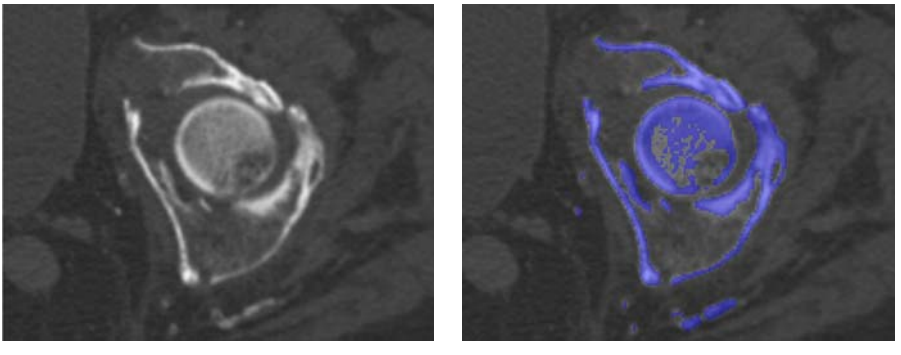

Fig. 1. Fractured left acetabulum in a case with osteopenic bone (left). Result of cortical bone segmentation step (right).

2 Related Work

Several methods have been proposed for the separation of bone components. Kang et al. [6] used a manually positioned sphere to separate the femoral head from the acetabulum, while Zoroofi et al. [7] introduced an involved automatic algorithm to fit a 3D ellipse to the femoral head. Statistical shape models have been applied successfully for the automatic segmentation of the intact pelvic and femoral bones from medical image data [8, 9]. But a priori knowledge from such models is very difficult to use in the segmentation of bone fragments because of the diversity of acetabular fractures [10] with often significant fragment displacements. Wang et al. [11] proposed the use of brittle fracture mechanics based on external stress and the internal intensity gradients for the partitioning of images. Cracks form when the mechanical stress exceeds a threshold that is governed by material properties. While there is an intuitive link to the separation of bone fragments, the solution would be expensive to compute for volumetric datasets. Also the authors showed that their segmentation

results are very sensitive to parameter settings such as the window size of stress distribution calculation.

3 Segmentation Pipeline

In the following the individual steps of the complete segmentation pipeline will be introduced in detail. The segmentation was based on CT scans of acetabular fractures. Images were reconstructed with a 512x512 matrix and a slice thickness of 2mm.

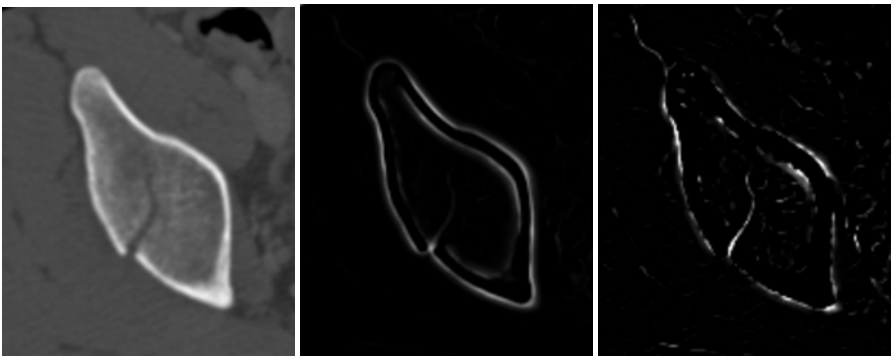

Fig. 2. Axial view of incomplete fracture above right hip joint (left). Original sheetness measure of non-inverted image (middle). New sheetness measure (right).

Segmentation of cortical bone. Simple thresholding of the CT images usually yields dissatisfying results. The CT signal of thin cortical bone sheets is blurred by partial volume effects. In addition, the quantitative accuracy of the signal is decreased by noise. For the segmentation of the cortical bone we therefore applied the adaptive thresholding scheme $t(x) = t_0 - \alpha\, c_{sheet}(x)$ to the input dataset, with $c_{sheet}(x)$ the sheetness measure proposed in [12] and α a weight factor. The method is based on the eigenvalues of the Hessian matrix computed for voxels of the intensity-inverted image at different scales. The scales should cover the range of considered structure sizes. In our case, four different scales Ω={0.75mm, 1.0mm, 1,5mm, 3mm} were chosen.

Applying the sheetness measure generates some false positive candidates at the skin surface, along the CT table, and at the wall of air-filled bowel loops. These false positives were masked by thresholding background air in the original dataset and enlarging the segmented region by morphological dilation. The resulting segmentation is shown for an example case with osteopenic bone in Figure 1.

Segmentation of cancellous bone. Based on the cortical bone segmentation, region growing was applied to the input dataset using the adaptive threshold $t(x) = t_0 + \beta\, c_{min}(x)$, with $c_{min}(x)$ a new minimum sheetness measure and β a weight factor. Just taking the standard sheetness measure of the non-intensity-inverted images to detect the structures results in significant false positive signals at locations with high intensity gradients, e.g. at the boundaries on both sides of the cortical bone (see Figures 2).

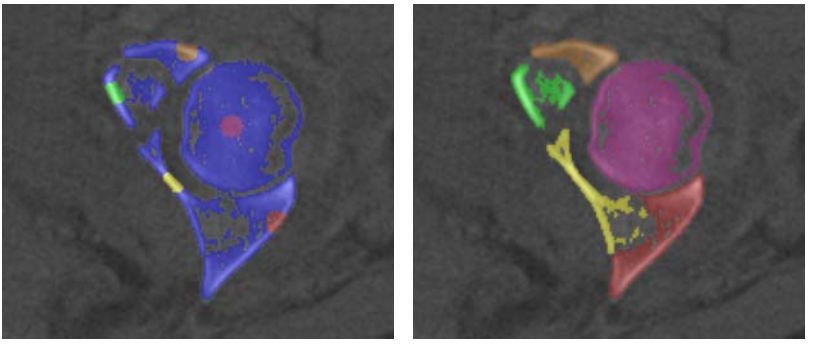

Fig. 3. User seeds added to bone labeling (left). Separated bone fragments using graph cut approach (right).

The new scheme reduces leakage of the segmentation into fracture gaps and joint spaces. Also, the true positives show a low contrast compared to the false positives. In order to reduce the false positive signal we propose a new measure analogous to the standard approach, based on a modification of the Hessian matrix:

$$H_{\min} = \begin{bmatrix} I_{xx} - |I_x| & |I_{xy}| & |I_{xz}| \\ |I_{xy}| & I_{yy} - |I_y| & |I_{yz}| \\ |I_{xz}| & |I_{yz}| & I_{zz} - |I_z| \end{bmatrix} \quad (1)$$

where the I_j and I_{jk} are first and second spatial derivatives of the voxel intensities. For the diagonal elements the false positive signal is reduced at edges by subtracting the absolute value of the gradient. Taking the absolute value of the off-diagonal elements fixes them at high positive values for minimum sheets independent of orientation.

Our new minimum sheetness measure increases the contrast of true positives compared to false positives significantly as can be seen in Figure 2 (right). However, it still generates some false positives, e.g. at low density fat tissue layers between bones and muscles. These are taken care of in the next steps.

Separation of bone fragments. The resulting segmentation of the cortical and cancellous bone is a binary partitioning into bone and background. The task of the following steps is to separate the different components. First a simple and fast 3D connected component labeling algorithm [13] is applied. Connected components smaller than 10mm^3 are rejected, representing the minimum size of objects of interest for clinical purposes. In addition, this step also removes small false positive labeled structures.

Unfortunately, between some fragments the boundaries are weak. Their labelings are not separable by a simple connected component algorithm. Therefore, we use graph cuts [14, 15]. This technique provides an energy minimization allowing efficient computation of a globally optimal image segmentation. For the algorithm a smoothness cost function $F_{p,q}(L_p,L_q)$ has to be defined, which gives the cost of assigning a node p to label L_p and the neighboring node q to a different label L_q. We have derived a modified function that pushes the cut surface towards low density structures showing a high minimum sheetness measure:

$$F_{p,q}(L_p, L_q) = \alpha\left(1 - e^{-\frac{I_p + I_q}{2}}\right) + \beta e^{-\frac{c_{\min}(p) + c_{\min}(q)}{2}} \quad (2)$$

where L_k, I_k, and $c_{\min}(k)$ are label, normalized intensity, and minimum sheetness value of node k. The influence of the sheetness and intensity terms can be controlled by parameters α and β, respectively. In our case both parameters were set to 0.5.

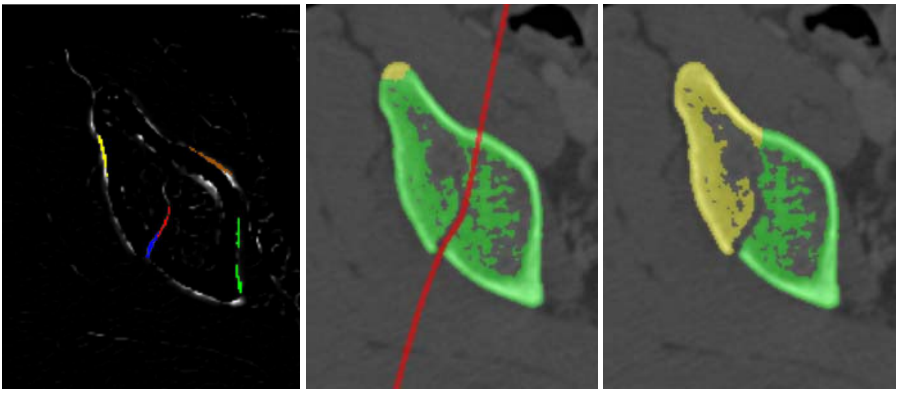

Fig. 4. Detected planes in right pelvic bone (color encoded). True positive fracture planes in blue & red (left). Cross section of TPS based on fracture gap plane (midde). Bone fragments correctly separated along surface after TPS refinement (right).

In order to carry out the graph cut based segmentation, seeds have to be added by a user to each bone fragment in the CT dataset on axial slices or multiplanar reformations. Figure 3 shows multiple bone fragments around the hip joint with user added seeds, as well as the resulting segmentation after applying the graph cut based separation.

Treatment of incomplete fractures. Unfortunately, incomplete fractures of the pelvic bone are quite common. The previously described graph cut technique then usually fails, since a cut into the non-fractured bone is expensive according to the smoothness cost function defined in Equation 2. Therefore, we propose an automated method for detection of incorrect bone fragment separation. The key idea is to first detect fracture planes in Hessian filtered images using an optimized Ransac algorithm [16], and then to use the detected planes as an initial estimate of a fracture surface that will be extended into the non-fractured part of the bone.

The input to the algorithm is a point cloud, corresponding to voxels in the image dataset showing a minimum sheetness measure exceeding a pre-defined threshold. Point normals are derived from the sheetness isosurface. The Ransac algorithm finds plane primitives exceeding a minimum size. Random sampling is performed at different localization scales using an octree implementation. These extracted planes are then used to detect incorrect separations of the graph cut step. A true positive fracture gap plane may be located in between two differently labeled, and therefore correctly separated voxel domains. An incorrect bone fragment separation is indicated by a

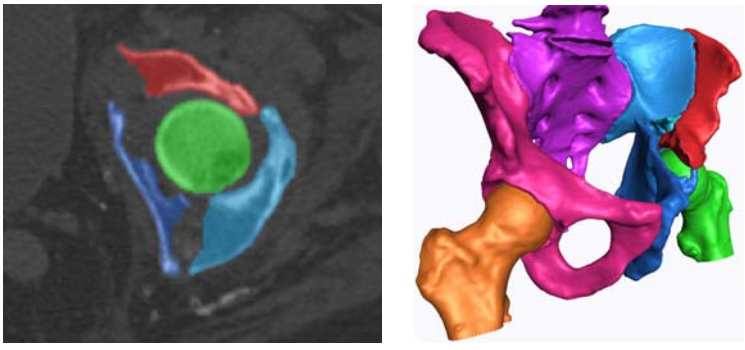

Fig. 5. Final segmentation after refinement of bone fragment contours (left). Surface mesh obtained from segmentation of this example case (right).

plane that is lined by equally labeled voxels on both sides. Finally, any false positive planes exhibit bone-labeled voxels only on one side. An image space method exploiting the graphics hardware was used to differentiate between these cases. Voxel volumes on both sides of a fracture gap plane are considered for an adjacency test. This test is carried out by projecting bone-labeled voxels of the segmented fragment in one such volume at a time onto a plane and testing for overlap in the framebuffer.

A plane is considered for resolving an incorrect bone fragment separation if the overlap is larger than a pre-defined threshold.

The algorithm for fracture gap plane detection produces a considerable number of false positives. These are located along low intensity fat tissue layers lining the cortical bone, in between two nearby and parallel cortical bone sheets, or in between muscles. The first two types of false positives can be filtered out by comparing them to a second set of planes detected in a point cloud derived from the standard sheetness measure of Descoteaux et al. [12] showing high signals at the cortical bone. False positives are then rejected based on a comparison of plane to plane orientations and distances in the two sets as well as testing for overlap using an image space method again. A complete detected set is shown for an example in Figure 4 (left). The planes remaining after the false positive elimination are colored in red and blue.

After removing all false positives, a thin plate spline surface [17] interpolating the constraining points of the true positive candidates is used as an initial estimate of a cut surface resolving the separation. The user may refine the thin plate spline by adding additional constraining points. The bone fragments are then separated along the accepted cut surface (see Figure 4)).

Segmentation refinement. In regions with low bone density, especially in the cancellous bone, the segmentation is still incomplete. This leads to artificial holes in the bone-labeling as well as in open regions (see Figure 4 (right)). In our case, the boundaries of bone fragments are at least partly lined by cancellous bone leading to sometimes quite large segmentation errors. We apply another graph cut based approach to solve both problems at the same time. The key idea is to build a graph from a volume of interest around the fragment currently considered for refinement. Another

suitable smoothness cost function that pushes the boundary towards the true fragment outline has been derived:

$$F_{q,p}\left(L_p, L_q\right) = \alpha e^{-\left|I_p - I_q\right|^2} + \beta\left(1 - e^{-\frac{d_f(p)+d_f(q)}{2}}\right) \tag{3}$$

where L_k and I_k, are label and normalized intensity of node k. The minimum distance of node k to voxels of the object is given by $d_f(k)$. Weighting parameters α and β were again set to 0.5. A minimum enclosing axis-aligned bounding box (AABB) padded by 10mm wide margins on all sides was taken as the volume of interest around the object. This segmentation step did not require any user input as the initialization can be obtained from the bone-labelings of the previous steps. The final segmentation result after refinement of bone fragment contours is depicted in Figure 5 (left). The mesh generated from the segmentation is shown in Figure 5 (right).

4 Results

The presented segmentation pipeline was applied in a pilot study to seven clinical cases with complex pelvic fractures involving the acetabulum. The system was used by an expert radiologist. Segmentation times were measured for each step separately and the overall time was computed (see Table 1).

Table 1. Performance time measurements in seconds

Step/Patient	A	B	C	D	E	F	G
1. Cortical bone	79	62	64	74	65	59	69
2. Cancellous bone	19	15	17	18	16	14	18
3. Connected component	4	3	3	4	3	3	3
4a. Separation (graph cut)	212	254	118	201	263	140	127
4b. Separation (spline)	203	211	-	-	206	-	-
5. Contour refinement	54	48	36	39	47	31	34
Overall	359	339	238	336	337	247	251

All cases could be successfully segmented. Note that steps 1, 2, 3 and 5 are carried out automatically, while in step 4a and 4b user interaction, e.g. placement of seeds in the bone fragments is required. Only cases A, B, and E had incomplete fractures, thus step 4b only had to be carried out for these. All but one segmentation yielded excellent results. Only case G required some additional manual refinement due to an anterior column bone fragment that was focally impacted onto the femoral head.

5 Conclusions

We have presented a semi-automatic multi-step segmentation method for the fractured pelvis. The segmentation of bone using local structure enhancement filtering is

followed by graph cut based separation of connected components. The key contribution is a technique for automated detection of incorrect bone fragment separation in the case of incomplete pelvic fractures. Additionally we propose a new sheetness measure based on properties of a modified Hessian matrix. This measure enhances minimum sheet-like structures such as fracture gaps and joint spaces.

In a first evaluation with seven clinical CT datasets of complex pelvic fractures our system was able to segment the bone fragments within four to six minutes in all cases, with only minimal user interaction.

References

1. Dakin, G.J., et al.: Acetabular fracture patterns: associations with motor vehicle crash information. J. Trauma 47(6), 1063–1071 (1999)
2. Vanderschot, P.: Treatment options of pelvic and acetabular fractures in patients with osteoporotic bone. Injury 38(4), 497–508 (2007)
3. Citak, M., et al.: Virtual 3D planning of acetabular fracture reduction. J. Orthop. Res. 26(4), 547–552 (2008)
4. Cimerman, M., Kristan, A.: Preoperative planning in pelvic and acetabular surgery: the value of advanced computerised planning modules. Injury 38(4), 442–449 (2007)
5. anonymous
6. Kang, Y., Engelke, K., Kalender, W.A.: A new accurate and precise 3-D segmentation method for skeletal structures in volumetric CT data. IEEE Trans. Med. Imaging 22(5), 586–598 (2003)
7. Zoroofi, R.A., et al.: Automated segmentation of acetabulum and femoral head from 3-D CT images. IEEE Trans. Inf. Technol. Biomed. 7(4), 329–343 (2003)
8. Lamecker, H., et al.: A 3D statistical shape model of the pelvic bone for segmentation. In: Medical Imaging 2004: Image Processing, Pts 1-3, vol. 5370, pp. 1341–1351 (2004)
9. Pettersson, J., et al.: Volume Morphing for Segmentation of Bone from 3D Data. In: Proceedings of the SSBA Symposium on Image Analysis (2005)
10. Letournel, E.: Acetabulum fractures: classification and management. Clin. Orthop. Relat. Res. (151), 81–106 (1980)
11. Wei, W., Ronald, C.: Image segmentation via brittle fracture mechanics. In: International Conference on Image Processing, 2004. ICIP (2004)
12. Descoteaux, M., et al.: Bone enhancement filtering: application to sinus bone segmentation and simulation of pituitary surgery. Comput. Aided Surg. 11(5), 247–255 (2006)
13. Beare, R.: Optimization of connected component labelling. The Insight Journal (2006)
14. Greig, D.M., Porteous, B.T., Seheult, A.H.: Exact maximum a posteriori estimation for binary images. Journal of the Royal Statistical Society. Series B, 271–279 (1989)
15. Boykov, Y., Jolly, M.-P.: Interactive Organ Segmentation Using Graph Cuts. In: Delp, S.L., DiGoia, A.M., Jaramaz, B. (eds.) MICCAI 2000. LNCS, vol. 1935, pp. 276–286. Springer, Heidelberg (2000)
16. Schnabel, R., Wahl, R., Klein, R.: Efficient RANSAC for Point-Cloud Shape Detection. Computer Graphics Forum 26(2), 214–226 (2007)
17. Bookstein, F.L.: Principal warps: thin-plate splines and the decomposition of deformations. IEEE Transactions on Pattern Analysis and Machine Intelligence 11(6), 567–585 (1989)